MECSOL 2019 - Proceedings of the7th International Symposium on Solid Mechanics,
V. Tita, A. Ferreira, M.L. Ribeiro, A. Vieira and A.T. Beck(Editors), ABCM, Sao Carlos, SP, Brazil, April15th to 17th, 2019

A Finite Element Model for Aeroelastic Analysis of Elongated Composite Plate-Like Wings

Gefferson C. Silva[1], Maurício V. Donadon[1], Flávio J. Silvestre[1], and Alessandro Guimarães[2]

[1] Department of Aeronautics, Instituto Tecnológico de Aeronáutica, Brazil

[2] Lightweight Structures Laboratory, Instituto de Pesquisas Tecnológicas, Brazil

Abstract: In recent years, fiber-reinforced composites have been increasingly used in the aeronautical field to improve the structural efficiency and reduce the weight of the aircraft. Furthermore, in order to enhance the aerodynamic performance, aircraft with highly elongated wings have been also extensively investigated. Within this context, this work presents a beam finite element model for aeroelastic analysis of elongated plate-like wings made of composite material. For validation purposes, a concentrated mass has been added to the model and modeled as a ballast located at the wing tip. A parametric study in terms of aeroelastic stability (flutter speed) has been carried out varying the positions of the ballast along the chordwise direction for different layup configurations.

Keywords: aeroelasticity, composite structures, f.e.m., aeroelastic optimization

INTRODUCTION

In order to improve the aerodynamic and structural performances, increase the flight envelope of the aircraft, and still reducing the weight, the aeronautical industry has been studying the application of composite materials and aircraft with more elongated wings in the last decades. These reasons motivate the interest into the study of flexible structures applied for aircraft.

Aircraft such as HELIOS developed by NASA (Noll et. al, 1999) and X-HALE developed by University of Michigan (Cesnik et. al., 2012) were designed with the objective of better understanding the dynamics of high flexible aircraft, where the interaction between structural dynamics and aerodynamics is stronger.

Among the current airliners in operation around the world, there are many examples of aircraft with moderate flexibility, such as the Boeing 787 and the Airbus A-380, the last one with vibration modes below 1 Hz. In addition, the Boeing 787 has about 50% of composite materials in its composition (Wright and Cooper, 2015).

Due to this fact, several works in the field of aeroelastic stability of composite structures have been published in recent decades. In many of these studies, the structural model was that of a beam-like wing, and the bend-twist deformation coupling for different aspects was performed, but most of them are concerned to avoid and/or suppress the flutter occurrence.

The flutter phenomenon can be considered as the most discussed and studied dynamic problem due the possible catastrophic effects related to it. In addition, in aircraft with increased airframe flexibility such as those with wing manufactured with composite materials, the interaction between aerodynamic and structural dynamics is typically stronger, increasing the possibility of flutter occurrence (Bisplinghoff and Ashley, 2013).

Shirk and Weisshaar (1986) shows the historical background of the use of composite materials into aircraft projects in order to control the aeroelastic deformation. Weisshaar (1981) gives a background and fundamental aspects about aeroelastic tailoring to enhance the performance of flexible fixed aircraft. Cesnik (1996) shows an aeroelastic analysis for elongated composite wings, and the main aspect approached in the paper is the importance of computing the right material couplings for aeroelastic stability.

In a recent study, Donadon and Faria (2016) investigate the aeroelastic stability boundary of flutter in Shape Memory Alloy Hybrid Composite laminates (SMAHC), which consists of SMAs wires and continuous carbon fibers embedded into a polymeric matrix resulting in a three constituent composite material.

In the present study, a linear composite beam finite element model of a high-aspect-ratio wing with a ballast located at the tip is developed to determine the aeroelastic stability (flutter and divergence) for different ply angles and different ballast positions along the chord-wise direction. Strip theory in the time-domain is used to compute the aerodynamic loads distribution. Finally, the aeroelastic analysis for each case are performed verifying the eigenvalues of the state matrix.

THE PLATE-LIKE WING

A rectangular composite plate for emulating the effects of an elongated flexible wing is analyzed in this work. For this, the plate has 350 mm long, 40 mm wide, and 6 layers with a total thickness of 1.14 mm, as shown in Fig. 1.

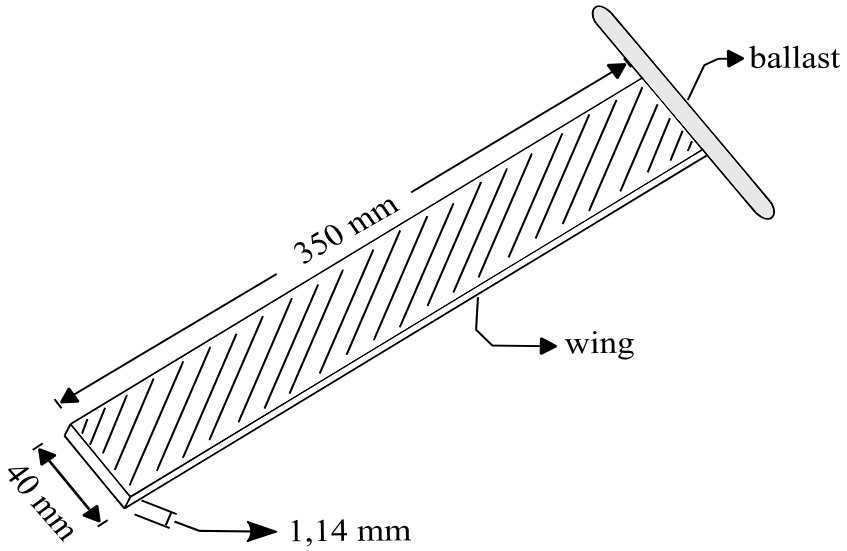

Figure 1: Plate-like wing with a ballast at the tip.

The composite material used here is a Tape AS4/8552 Carbon Epoxy with mechanical properties as shown in Table 1. The ballast is a slender body with 0.035 kg mass and moments of inertia I_{xx} and I_{yy} equal to 1.858×10^5 kgm². In addition, the ballast may be moved toward the leading or trailing edges to verify the effects of different inertia couplings on the aeroelastic stability of the wing.

Table 1: Mechanical proprieties of the AS4/8552 Carbon Epoxy.

Layer Propriety	Value	Units
t	0.19	mm
ρ	1500	kg/m³
E_1	129.5	GPa
E_2	9.37	GPa
υ_{12}	0.38	-
G_{12}	5.24	GPa

AEROELASTIC FORMULATION

Structural Model

The Bernoulli-Euler beam theory works very well for structural elements modeling under pure bending loads with 2 degrees of freedom, the vertical displacement and the rotation of the cross-section, just as shown in Fig. 2.

The system we are looking for modeling is an elongated rectangular flat plate that represents a flexible wing. Therefore, with the interest of describing the aeroelastic behavior of the wing modeled as an Euler-Bernoulli beam, we should to incorporate an additional degree of freedom to account the torsion around the longitudinal axis. In order to remain the cross-section plane, the deformations along the width and thickness directions are neglected for the torsion modeling, considering only the torsional angle and the vibration dynamics related to it.

The element of length a has six degrees of freedom (3 per node) referred to a global coordinates *xyz*. In a vector form, the degrees of freedom are

$$\boldsymbol{q}^e = \{h_1 \quad \gamma_1 \quad \theta_1 \quad h_2 \quad \gamma_2 \quad \theta_2\}^T \tag{1}$$

where h is the vertical displacement, γ is the rotation of the cross-section, and θ is the torsion around thelongitudinal axis.

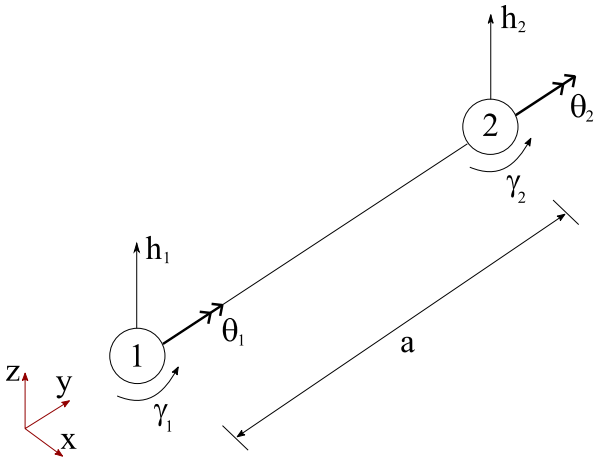

Figure 2: Beam element with six degrees of freedom.

In order to satisfy the continuity requirements, a cubic Hermitian shape function is used for the vertical displacement and a linear one for the torsional displacement,

$$\begin{cases} H_1(\xi) = \frac{1}{4}(1-\xi)^2(2+\xi) \\ H_2(\xi) = \frac{a}{2}\frac{1}{4}(1-\xi)^2(\xi+1) \\ H_3(\xi) = 0 \\ H_4(\xi) = \frac{1}{4}(1+\xi)^2(2-\xi) \\ H_5(\xi) = \frac{a}{2}\frac{1}{4}(1+\xi)^2(\xi-1) \\ H_6(\xi) = 0 \end{cases} \quad \begin{cases} L_1(\xi) = 0 \\ L_2(\xi) = 0 \\ L_3(\xi) = \frac{1}{2}(1-\xi) \\ L_4(\xi) = 0 \\ L_5(\xi) = 0 \\ L_6(\xi) = \frac{1}{2}(1+\xi) \end{cases} \tag{2}$$

The interpolated approximations for h, γ and θ are given by

$$h = \sum_{i=1}^{6} H_i q_i^e = \boldsymbol{N_h q^e}, \quad \gamma = \sum_{i=1}^{6} H_i' q_i^e = \boldsymbol{N_\gamma q^e}, \quad \theta = \sum_{i=1}^{6} L_i q_i^e = \boldsymbol{N_\theta q^e} \tag{3}$$

The generalized displacements $\boldsymbol{\Delta} = \{h \quad \gamma \quad \theta\}^T$ can still be written in the follwing matrix form in terms of the nodal displacements $\boldsymbol{q^e}$

$$\boldsymbol{\Delta} = [\boldsymbol{N_h} \quad \boldsymbol{N_\gamma} \quad \boldsymbol{N_\theta}]^T \boldsymbol{q^e} = \boldsymbol{N q^e} \tag{4}$$

where $\boldsymbol{N}$ is the interpolation matrix and dependent only on space, while the vector $\boldsymbol{q^e}$ is dependent on time. Thus, the generalized velocity vector $\dot{\boldsymbol{\Delta}}$ is given by

$$\dot{\boldsymbol{\Delta}} = \boldsymbol{N \dot{q}^e} \tag{5}$$

The finite element method used to model the behaviour of the wing is based on energy principles. For a single element, the kinetic energy neglecting membrane effects is given by

$$T_e = \frac{1}{2}\rho \int_e \dot{\boldsymbol{\Delta}}^2 \, dV \tag{6}$$

where ρ is the density of the material.

When Eq. (5) is substituted into Eq. (6), the kinetic energy in terms of nodal degrees of freedom is

$$T_e = \frac{1}{2}\boldsymbol{\dot{q}^{eT}}\left[\rho \int_e \boldsymbol{N^T N} \, dV\right]\boldsymbol{\dot{q}^e} \tag{7}$$

The bracketed expression in Eq. (7) is the consistent element mass matrix $\boldsymbol{m^e}$, which can be rewritten as

$$\boldsymbol{m^e} = \rho A \frac{a}{2}\int_{-1}^{+1} \boldsymbol{N_h^T N_h} d\xi + \rho I \frac{a}{2}\int_{-1}^{+1} \boldsymbol{N_\gamma^T N_\gamma} d\xi + \rho J_\theta \frac{a}{2}\int_{-1}^{+1} \boldsymbol{N_\theta^T N_\theta} d\xi \tag{8}$$

where A is the cross-sectional area, I is the moment of inertia related to the rotational motion, and J_θ is the polar moment of inertia related to the torsional motion of the beam.

The strain energy for an element is composed by the contribution of bending and torsional displacements

$$U_e = \frac{1}{2}\int_e \boldsymbol{\sigma^T \epsilon} \, dV + \frac{1}{2}\int_e \boldsymbol{\tau^T \bar{\gamma}} \, dV \tag{9}$$

where $\boldsymbol{\epsilon}$ is the normal strain and $\boldsymbol{\bar{\gamma}}$ is the shear strain for thin wallet structures under torsion (Megson, 2013).

The constitutive equations assumed for the composite beam are given by

$$\begin{cases} \boldsymbol{\sigma} = \bar{E}\boldsymbol{\epsilon} \\ \boldsymbol{\tau} = \bar{G}\overline{\boldsymbol{\gamma}} \end{cases} \tag{10}$$

where $\bar{E}$ and $\bar{G}$ are the equivalent bending and shear moduli, respectively, for the composite beam (Kassapoglou, 2013).

Substituting Eq. (10) in Eq. (9), the element strain energy results

$$U_e = \frac{1}{2}\bar{E}\int_e \boldsymbol{\epsilon}^T\boldsymbol{\epsilon}\, dV + \frac{1}{2}\bar{G}\int_e \overline{\boldsymbol{\gamma}}^T\overline{\boldsymbol{\gamma}}\, dV \tag{11}$$

which results in

$$U_e = \frac{1}{2}\boldsymbol{q^e}^T\left[\bar{E}I\frac{8}{a^3}\int_{-1}^{+1}\boldsymbol{N}_{\boldsymbol{h},\xi\xi}^T\boldsymbol{N}_{\boldsymbol{h},\xi\xi}d\xi \;+\; \bar{G}J\frac{2}{a}\int_{-1}^{+1}\boldsymbol{N}_{\boldsymbol{\theta},\xi}^T\boldsymbol{N}_{\boldsymbol{\theta},\xi}d\xi\right]\boldsymbol{q^e} \tag{12}$$

where J is the torsion constant, and the expression between brackets is the element stiffness matrix given by

$$\boldsymbol{k^e} = \bar{E}I\frac{8}{a^3}\int_{-1}^{+1}\boldsymbol{N}_{\boldsymbol{h},\xi\xi}^T\boldsymbol{N}_{\boldsymbol{h},\xi\xi}d\xi \;+\; \bar{G}J\frac{2}{a}\int_{-1}^{+1}\boldsymbol{N}_{\boldsymbol{\theta},\xi}^T\boldsymbol{N}_{\boldsymbol{\theta},\xi}d\xi \tag{13}$$

The strain energy expressed in Eq. (12) neglects the warping effects by assuming warping displacements unimportant in aeroelastic analysis.

The total kinetic and strain energies for various elements are given by

$$\begin{cases} T \leftarrow \sum_e T_e = \;{}^1\!/_2\sum_e \dot{\boldsymbol{q}}^{\boldsymbol{e}^T}\boldsymbol{m^e}\dot{\boldsymbol{q}}^{\boldsymbol{e}} = {}^1\!/_2\,\dot{\boldsymbol{q}}^{\boldsymbol{T}}\boldsymbol{M}\dot{\boldsymbol{q}} \\ U \leftarrow \sum_e U_e = \;{}^1\!/_2\sum_e \boldsymbol{q}^{\boldsymbol{e}^T}\boldsymbol{k^e}\boldsymbol{q^e} = {}^1\!/_2\,\boldsymbol{q}^{\boldsymbol{T}}\boldsymbol{K}\boldsymbol{q} \end{cases} \tag{14}$$

where $\boldsymbol{q}$ is the global displacement vector, $\boldsymbol{M}$ is the global mass matrix, and $\boldsymbol{K}$ is the global stiffness matrix.

The inertia effects related to the ballast are accounted within the mass matrix of the element that represents the wing tip, accounting the first and second moments of inertia of the ballast. Furthermore, in order to be conservative in terms of aeroelastic stability, the structural damping is neglected in this work.

The equations of motion of the system can now be obtained from the set of equations expressed in Eq. (14), and applying the Hamilton's principle leads to

$$\int_{t_1}^{t_2}\delta(T-U)dt + \delta\int_{t_1}^{t_2}W^{aer}dt = 0 \tag{15}$$

where δ is the variational operator, and W^{aer} is the work done by aerodynamic loads ($\boldsymbol{F^{aer}}$), resulting in

$$\boldsymbol{M}\ddot{\boldsymbol{q}} + \boldsymbol{K}\boldsymbol{q} = \boldsymbol{F^{aer}} \tag{16}$$

Aerodynamic Model

A strip theory in time-domain based on Wagner's function (Silvestre and Luckner, 2015) was developed considering the number of strips equal to the number of elements, and the center of the strips located at the nodes of the elements, except for the first node, as can be seen in Fig. 3.

The aerodynamic loads for all strips can be written in a vector form

$$\boldsymbol{F^{aer}} = \left\{-l(y_1,t) \quad 0 \quad m^{ea}(y_1,t) \;\cdots\; -l(y_j,t) \quad 0 \quad m^{ea}(y_j,t) \;\cdots\; -l(y_n,t) \quad 0 \quad m^{ea}(y_n,t)\right\}^T \tag{17}$$

where n is the total number of strips, l is the lift, and m^{ea} is the moment for a given strip at the elastic axis.

Similarly to the typical section theory, assuming that there is no chord-wise deformation at the *j*-th strip, the loads are given by

$$\begin{Bmatrix} -l(y_j,t) \\ 0 \\ m^{ea}(y_j,t) \end{Bmatrix} = \left(\boldsymbol{a_1}(y_j)\begin{Bmatrix}\ddot{h}(y_j,t)\\ \ddot{\gamma}(y_j,t)\\ \ddot{\theta}(y_j,t)\end{Bmatrix} + \boldsymbol{a_2}(y_j)\begin{Bmatrix}\dot{h}(y_j,t)\\ \dot{\gamma}(y_j,t)\\ \dot{\theta}(y_j,t)\end{Bmatrix} + \boldsymbol{a_3}(y_j)\begin{Bmatrix}h(y_j,t)\\ \gamma(y_j,t)\\ \theta(y_j,t)\end{Bmatrix} + \boldsymbol{a_4}(y_j)\begin{Bmatrix}\lambda_1(y_j,t)\\ \lambda_2(y_j,t)\end{Bmatrix}\right)\Delta y_j \tag{18}$$

wherein $\lambda_1(y_j,t)$ and $\lambda_2(y_j,t)$ represent the lag states at the *j*-th strip, and can be determined by the following differential equations

$$\begin{Bmatrix}\dot{\lambda}_1(y_j,t)\\ \dot{\lambda}_2(y_j,t)\end{Bmatrix} = \boldsymbol{b_1}(y_j)\begin{Bmatrix}\ddot{h}(y_j,t)\\ \ddot{\gamma}(y_j,t)\\ \ddot{\theta}(y_j,t)\end{Bmatrix} + \boldsymbol{b_2}(y_j)\begin{Bmatrix}\dot{h}(y_j,t)\\ \dot{\gamma}(y_j,t)\\ \dot{\theta}(y_j,t)\end{Bmatrix} + \boldsymbol{b_3}(y_j)\begin{Bmatrix}h(y_j,t)\\ \gamma(y_j,t)\\ \theta(y_j,t)\end{Bmatrix} + \boldsymbol{b_4}(y_j)\begin{Bmatrix}\lambda_1(y_j,t)\\ \lambda_2(y_j,t)\end{Bmatrix} \tag{19}$$

where $\boldsymbol{a_{1,\ldots 4}}$ and $\boldsymbol{b_{1,\ldots 4}}$ are the aerodynamic matrices related to each strip.

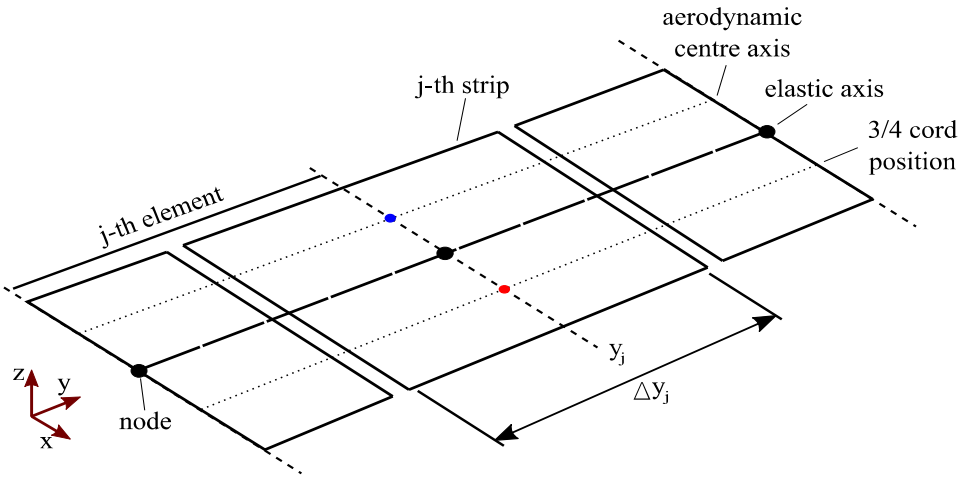

Figure 3: Strips discretization schematic.

In order to compute the 3D aerodynamic effects, the strip theory was modified (Yates, 1966) to predict the lift distribution over the wing, as shown in Fig. 4. For that, the reduction of the lift towards the tip is achieved by assuming the following exponential approximation for the lift–curve slope C_{l_α} at each strip.

$$C_{l_\alpha}(y_j) = 2\pi\left[1-\left(\frac{y_j}{span}\right)^3\right] \tag{20}$$

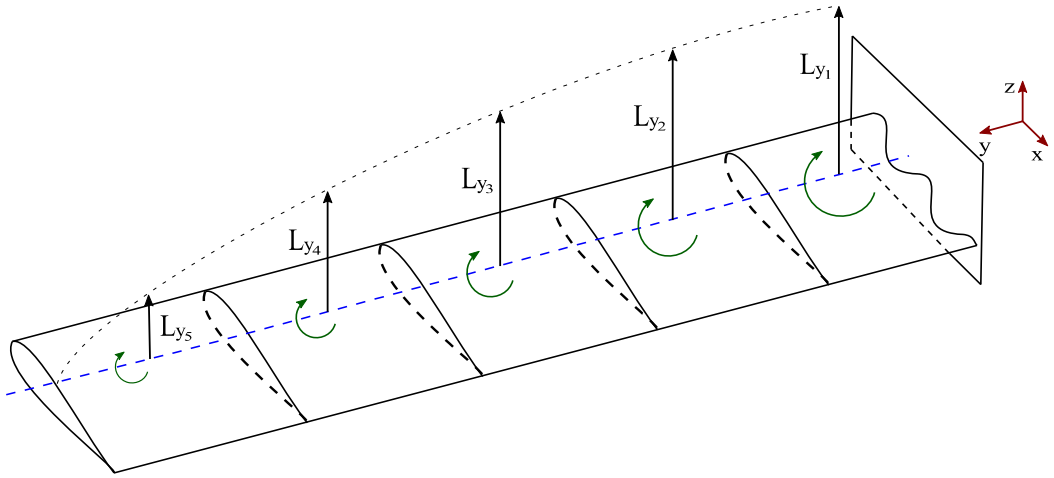

Figure 4: Spanwise lift distribution for a realistic wing and strip theory model.

Considering the lift distribution above, the aerodynamic loads and the lag states for the complete lifting surface can be written in global coordinates in a matrix form,

$$\begin{aligned} \boldsymbol{F^{aer}} &= \boldsymbol{A_1}\,\ddot{\boldsymbol{q}} + \boldsymbol{A_2}\dot{\boldsymbol{q}} + \boldsymbol{A_3}\,\boldsymbol{q} + \boldsymbol{A_4}\,\boldsymbol{\lambda} \\ \dot{\boldsymbol{\lambda}} &= \boldsymbol{B_1}\,\ddot{\boldsymbol{q}} + \boldsymbol{B_2}\dot{\boldsymbol{q}} + \boldsymbol{B_3}\,\boldsymbol{q} + \boldsymbol{B_4}\,\boldsymbol{\lambda} \end{aligned} \tag{21}$$

in which $\boldsymbol{A_{1,\dots 4}}$ and $\boldsymbol{B_{1,\dots 4}}$ are the global aerodynamic matrices, and $\boldsymbol{\lambda}$ is the global lag states vector.

Then, we can write the equations of motion in a state-space form from Eqs. (16) and (21), and the trivial solution $\boldsymbol{I\dot{q}} = \boldsymbol{I\dot{q}}$, resulting in

$$\begin{Bmatrix} \dot{\boldsymbol{q}} \\ \ddot{\boldsymbol{q}} \\ \dot{\boldsymbol{\lambda}} \end{Bmatrix} = \begin{bmatrix} \boldsymbol{0}_{3n\times 3n} & \boldsymbol{I}_{3n\times 3n} & \boldsymbol{0}_{3n\times 2n} \\ -\bar{\boldsymbol{M}}^{-1}\bar{\boldsymbol{K}} & \bar{\boldsymbol{M}}^{-1}\boldsymbol{A_2} & \bar{\boldsymbol{M}}^{-1}\boldsymbol{A_4} \\ \boldsymbol{B_3} - \boldsymbol{B_1}\bar{\boldsymbol{M}}^{-1}\bar{\boldsymbol{K}} & \boldsymbol{B_2} + \boldsymbol{B_1}\bar{\boldsymbol{M}}^{-1}\boldsymbol{A_2} & \boldsymbol{B_4} + \boldsymbol{B_1}\bar{\boldsymbol{M}}^{-1}\boldsymbol{A_4} \end{bmatrix} \begin{Bmatrix} \boldsymbol{q} \\ \dot{\boldsymbol{q}} \\ \boldsymbol{\lambda} \end{Bmatrix} \tag{22}$$

or just,

$$\dot{\boldsymbol{Q}} = \boldsymbol{AQ} \tag{23}$$

where $\bar{\boldsymbol{M}} = \boldsymbol{M} - \boldsymbol{A_1}$ is the total mass matrix, $\bar{\boldsymbol{K}} = \boldsymbol{K} - \boldsymbol{A_3}$ is the total stiffness matrix, $\boldsymbol{Q}$ is the state vector, and $\boldsymbol{A}$ is the dynamic matrix.

AEROELASTIC ANALYSIS

The aeroelastic analysis has been obtained by analysing the eigenvalues of the dynamic matrix. For an oscillatory system, the eigenvalues $\boldsymbol{\Lambda}$ of the dynamic matrix $\boldsymbol{A}$ are in the form

$$\Lambda_j = -\zeta_j \omega_j \pm i\omega_j \sqrt{1-\zeta_j^2}\,, j = 1, 2, \ldots, N \tag{24}$$

and

$$\zeta_j = -\frac{Re(\Lambda_j)}{\omega_j} \tag{25}$$

where ω_j is the j-th natural frequency, and ζ_j is the j-th damping ratio. If the real part of the complex eigenvalue is positive, i.e., if any damping ratio is negative then the system is dynamically unstable (flutter). However, if the eigenvalue is real and positive the system becomes statically unstable (divergence).

For the system considered here, an investigation on how the flutter and divergence speeds change for different ply angles, which were considered laminates with six layers at the same orientation varying from 0° up to 90° with $\Delta\phi$ of 15°, and for each ply angle case different ballast positions along the chordwise direction were evaluated considering positions of ± 5 mm, ± 10 mm, and ± 15 mm with respect to the elastic axis. Both variations contribute to the vibration modes calculation, and consequently change the flutter speed. The divergence speed is not affected by the variation of the ballast position, because this is a static phenomenon.

Generally, the flutter phenomenon occurs at high speeds, i.e., at low angles of attack. Therefore, zero-angle-of-attack is considered as initial condition for all simulations, and for this, a V-g-ω diagram is used to obtain the flutter and divergence speeds. The structural and aeroelastic responses converge with only 5 elements, but all results were generated considering 1 element per centimeter along the spanwise direction, i.e., 35 elements were used for the analysis.

Figure 5 shows the V-g-ω diagram for a specific case with $\phi = 45°$ and $x_{SB} = -10$ mm. For this configuration, the divergence speed is 48.7 m/s and the flutter speed is 10.8 m/s as a consequence of the coupling of the first torsion mode (24.74 Hz) and the second bending mode (20.17 Hz).

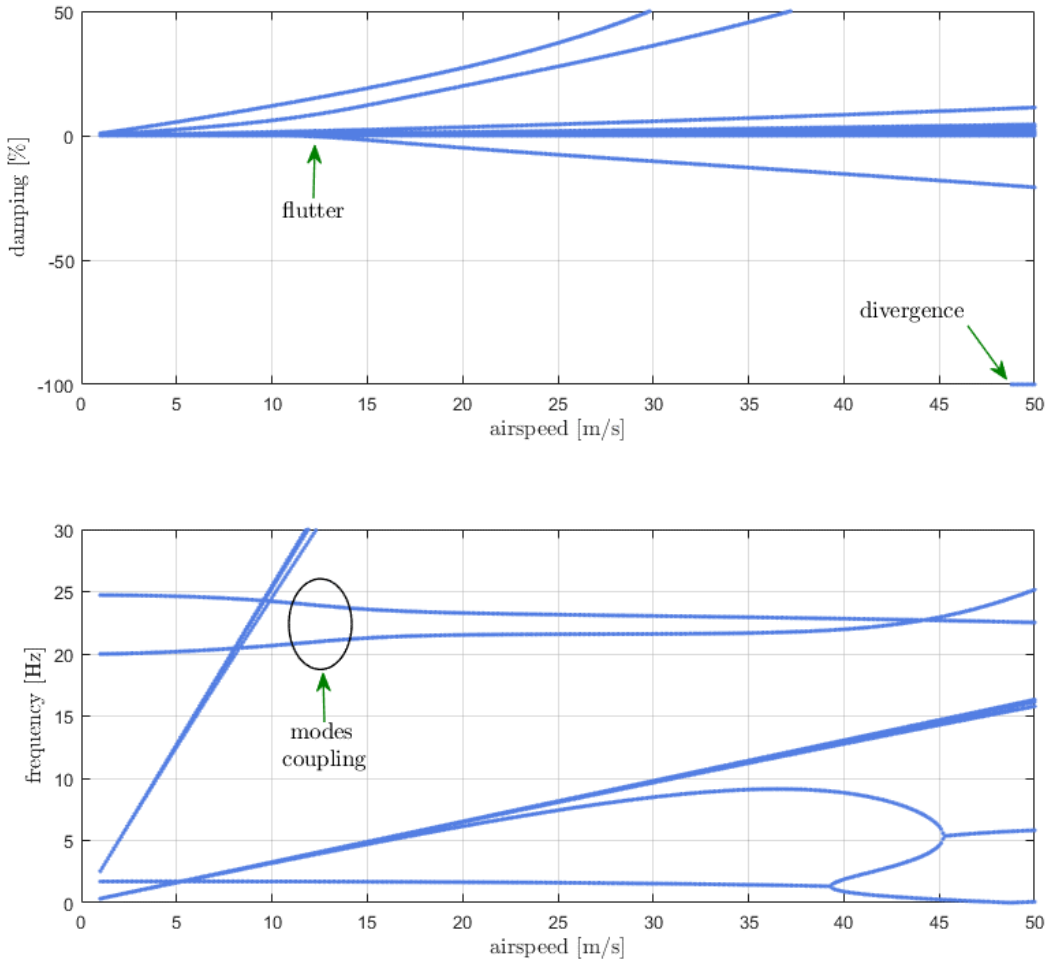

Figure 5: V-g-ω diagram for $\phi = 45°$ and $x_{SB} = -10$ mm.

In addition, Fig. 6 shows the numerical normalized lift-curve slope for each strip used to compute the aerodynamic loads. The lifting-line theory assumes that the lift distribution is based only on the wing geometry and flow conditions, where the maximum lift value is at the wing root, and moving toward the tip the lift becomes very small.

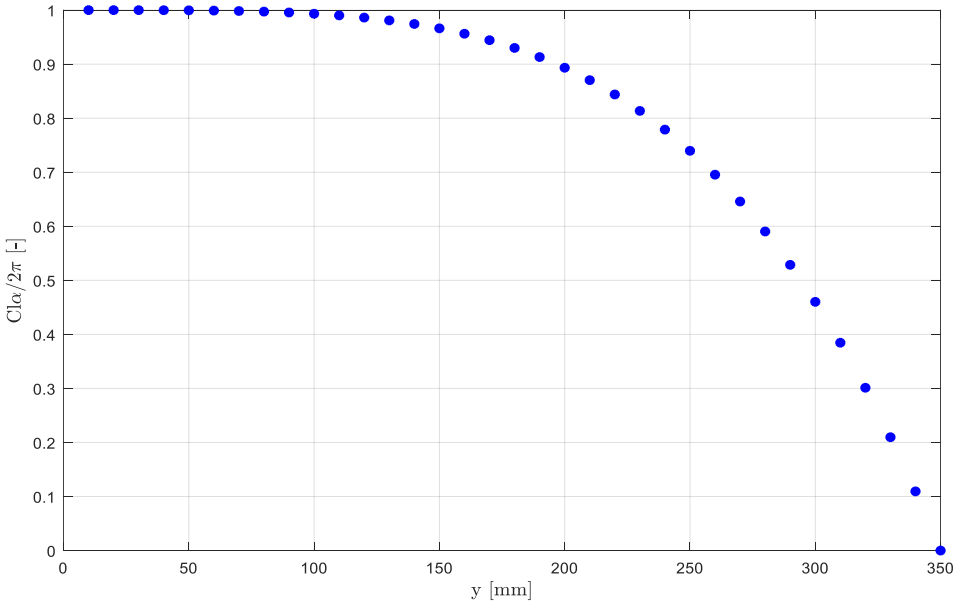

Figure 6: Numerical lift-slope distribution.

Figure 7 is a three-dimensional representation of how the flutter speed V_{fl} changes as a function of x_{SB} and ϕ. The maximum flutter speed found is $V_{fl} = 67.9$ m/s, and it is achieved when $\phi = 0°$ and $x_{SB} = -10$ mm, i.e., the configuration where the fiber orientation and the air stream direction are collinear and the ballast is located at the aerodynamic axis position. For this case, the ratio between the modes involved into the flutter is $\omega_{2°bending}/\omega_{1°torsion} = 0.30$. On the other hand, the minimum flutter speed occurs when $\phi = 90°$, $x_{SB} = -5$ mm, and $\omega_{2°bending}/\omega_{1°torsion} = 0.87$. According to Bismarck-Nasr (1999), in a binary flutter behaviour, as much closer the ratio between the modes frequencies are of the unity, the flutter speed decreases.

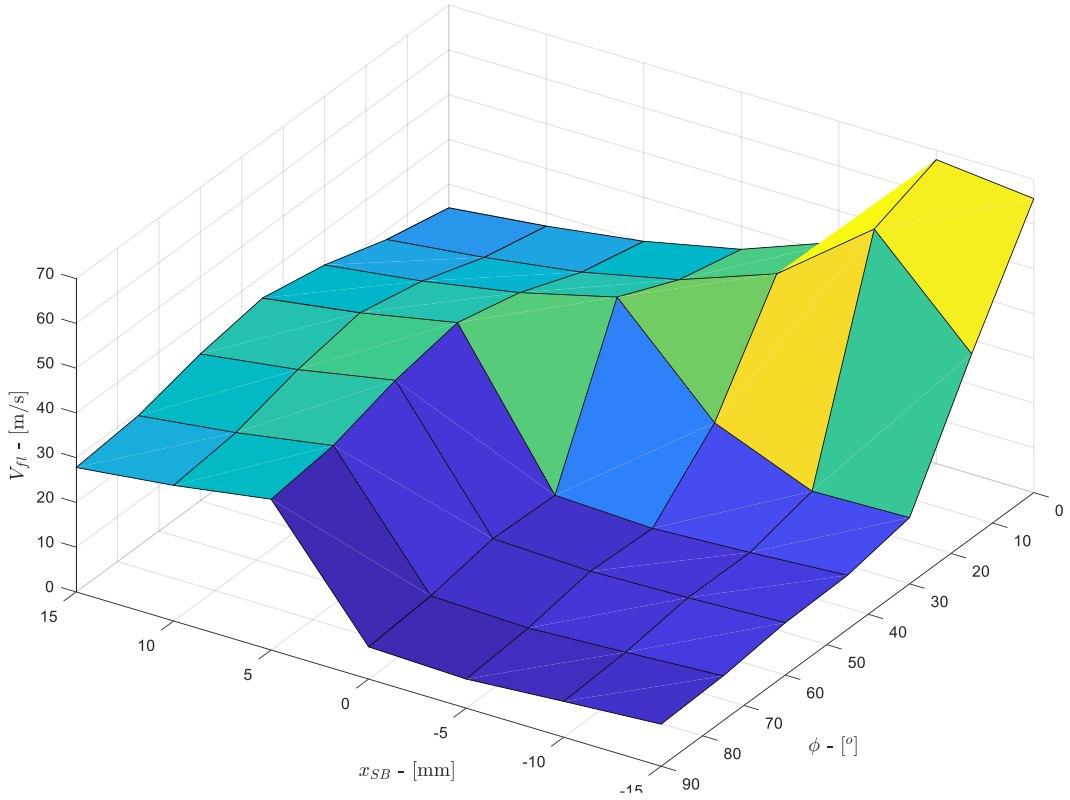

Figure 7: Variation of flutter speed with the ballast position and ply angle.

Considering the maximum and minimum flutter speeds, the set of configurations considered in this work result in a range of $\Delta V_{fl} = 61.4$ m/s. In addition, the results show that the lower flutter speed variation regarding to the different ply angles is when $x_{SB} = +15$ mm, where $\Delta V_{fl} = 10.4$ m/s.

For divergence, ply angles close to 45° produce more favourable bending-twist interaction in terms of equivalent structural stiffness and leading to higher divergence speeds, and for ply angles larger than 45° the divergence speeds start to decrease again, as can be seen in Fig. 8. All divergence speeds were computed looking at the V-g-f diagram in what speed the damping becomes negative and the frequency becomes zero.

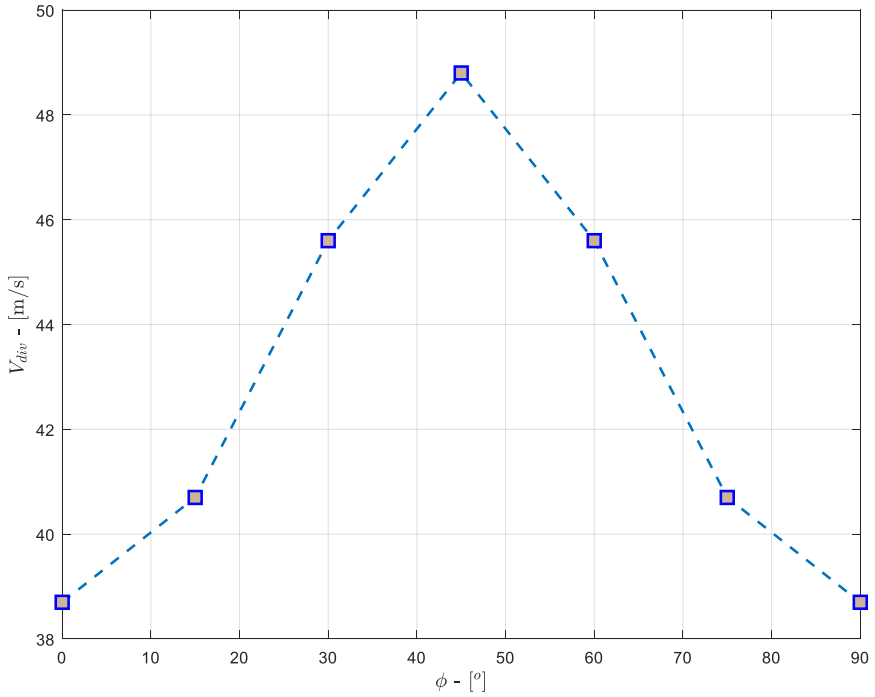

Figure 8: Variation of divergence speed with the ply angle variation.

CONCLUSIONS

The present work presented a finite element model of a high-aspect-ratio wing manufactured in composite material accounting the equivalent beam behaviour coupled to a time-domain strip theory aerodynamic model that accounts the 3D flow effects by using the exponential lifting-line approximation for the aeroelastic analysis.

The possibility of using composite materials to improve structural efficiency in the aircraft opens new possibilities, such as handling material couplings to induce the desired structural response and/or to avoid aeroelastic instabilities. As shown in this work, both flutter and divergence speeds can be altered by the material couplings, whether it is induced by the fiber orientation and/or by a concentrated mass. Despite this, many layup configurations were not evaluated in this work and can be used to obtain the desired structural and aeroelastic responses, such as cross-ply, angle-ply, and anti-symetric laminates.

Currently, aeroelastic optimization is an integral part of formal procedures for aircraft designers evaluate during many project phases of the aircraft. Then, this work moves toward one of the main research subjects addressed in the last years in aeronautical and special fields. More broadly, all of these proposed studies have the objective of making high flexible aircraft very efficient from the aeroelastic point of view in the next years.

ACKNOWLEDGEMENTS

This work has been funded by Brazilian agencies Coordenação de Aperfeiçoamento de Pessoal de Nível Superior - CAPES, Instituto de Pesquisas Tecnológicas do Estado de São Paulo S. A. – IPT, and by Fundação de Apoio ao Instituto de Pesquisas Tecnológicas do Estado de São Paulo – FIPT (grants Programa Novos Talentos).

REFERENCES

Bismarck-Nasr, M. N., 1999, “Structural Dynamics in eronautical engineering”. AIAA.

Bisplinghoff, R.L., and Ashley, H., , 2013, “Principles of Aeroelasticity”. Courier Corporation.

Cesnik, C. E. S. et. al., 2012, “XHALE: A Very Flexible Unmanned Aerial Vehicle for Nonlinear Aeroelastic Tests”, AIAA Journal, vol. 50, No. 12.

Cesnik, C., Hodges, D., & Patil, M., 1996, “Aeroelastic Analysis of Composite Wings”. In 37th Structure, Structural Dynamics and Materials Conference, p. 1444.

Donadon, M. V., & de Faria, A. R., 2016, “Aeroelastic Behavior of Composite Laminated Shells with Embedded SMA Wires Under Supersonic Flow”. Aerospace Science and Technology, 52, 157-166.

Kassapoglou, C., 2013, “Design and Analysis of Composite Structures: With Applications to Aerospace Structures”. John Wiley & Sons.

Megson, T. H. G., 2013, “Introduction to Aircraft Structural Analysis”. Butterworth-Heinemann.

Noll, T. E., et. al., “Investigation of the Helios Prototype Aircraft Mishap” [online article], http://www.nasa.gov/pdf/64317main_helios.pdf.

Shirk, M. H., Hertz, T. J., and Weisshaar, T. A., 1986, “Aeroelastic Tailoring - Theory, Practice, and Promise”, J. Aircraft, Vol. 23, No. 1, pp. 6-18.

Silvestre, F. J.; Luckner, R., “Experimental Validation of a Flight Simulation Model for Slightly Flexible Aircraft”. AIAA Journal, American Institute of Aeronautics and Astronautics, v. 53, n. 12, p. 3620-3636, 2015.

Weisshaar, T. A., 1981, “Aeroelastic Tailoring of Forward Swept Composite Wings”, J. Aircraft, Vol. 18, No. 8, pp. 669-676.

Wright, J. R., and Cooper, J. E., 2015, “Introduction to Aircraft Aeroelasticity and Loads”, Wiley, New York.

Yates, E.C., 1966, “Modified Strip Analysis Method for Predicting Wing Flutter at Subsonic to Hypersonic Speeds”. Journal of Aircraft, 3 (1), 25–29.

RESPONSIBILITY NOTICE

The authors are the only responsible for the printed material included in this paper.